

Supplementary Information

Visualizing asymmetric phase separation driven by surface ionic diffusion in lithium titanate

Yuki Nomura^{1,*}, Kazuo Yamamoto¹, Tsukasa Hirayama¹

¹Nanostructures Research Laboratory, Japan Fine Ceramics Center, 2-4-1 Mutsuno, Atsuta-ku, Nagoya, Aichi, 456-8587, Japan

*To whom correspondence: y_nomura@jfcc.or.jp

Table of Contents

- SI-1. Experimental
- SI-2. Area and method for visualizing the Li distribution in $\text{Li}_4\text{Ti}_5\text{O}_{12}$
- SI-3. Electron diffraction
- SI-4. Effect of electron irradiation
- SI-5. Change in Li distribution in another region.
- SI-6. References

SI-1. Experimental

Fabrication of the solid-state Li-ion battery

Commercially available $\text{Li}_4\text{Ti}_5\text{O}_{12}$ and LPS (PO0119, MSE Supplies LLC) were used as the active material and SE, respectively. The ionic conductivity of LPS was approximately 1.0×10^{-3} S/cm at room temperature. A disc-shaped pellet with a diameter of 10 mm was prepared by compressing 50 mg of LPS in a cylindrical mold. Subsequently, a small amount of $\text{Li}_4\text{Ti}_5\text{O}_{12}$ particles were distributed on one side of the LPS pellet. This pellet was pressed under 300 MPa at 120 °C. A 150- μm -thick Li-In metal foil was placed on another side (as shown in **Fig. 1a**). The cell was assembled in an argon-filled glove box (GB) with a dew point below -70 °C. The $\text{Li}_4\text{Ti}_5\text{O}_{12}$ /LPS/In-Li pellet was removed from the cylindrical mold and transferred into an ion-beam sputtering system (Precision Etching Coating System 2, Gatan Inc.) to ensure no exposure to air during the deposition of the Pt current collector on the $\text{Li}_4\text{Ti}_5\text{O}_{12}$ particles. Detailed information on the fabrication of the solid-state battery cell can be found in the literature.¹

Charge and discharge measurements

Charge and discharge measurements shown in **Fig. 1c** were performed in the transmission electron microscope at a constant current (CC) of 300 nA followed by constant voltages (CV) of 0.4 and 1.6 V vs. In-Li using a potentiogalvanostat (SP-200, BioLogic Science Instruments, France). The charge–discharge measurement was terminated when the current reached ~ 10 nA.

FIB

The battery cell was loaded on an air-tight FIB holder inside the GB and then transferred to a FIB system (FB-2100, Hitachi High-Tech. Corp., Japan) without exposure to air to prevent the degradation of LPS. A segment of the $\text{Li}_4\text{Ti}_5\text{O}_{12}$ side was thinned using FIB accelerated at 40 kV with a probe current of less than 5 nA. The thinned region had a thickness of approximately 200 nm.

STEM-EELS

A 300-kV transmission electron microscope (JEM-ARM300F2 GRAND ARM2, JEOL Ltd., Japan) equipped with an EEL spectrometer (Gatan imaging filter (GIF) Continuum-K3, Gatan Inc., USA) was used for ADF-STEM, operando STEM-EELS, and 4D-STEM observations. The STEM-EELS data has a resolution of 178×158 pixels, and each pixel in **Fig. 2** and **3** has a dimension of 20 nm. The electron probe current was approximately 70 pA, the energy dispersion was 0.15 eV/pixel, and the exposure time was 0.01 s/pixel. Detailed information on the design of the vacuum transfer TEM holder with biasing electrodes can be found in the literature.²

SI-2. Area and method for visualizing the Li distribution in $\text{Li}_4\text{Ti}_5\text{O}_{12}$

The area and method for visualizing the Li distribution are shown in **Fig. S3**. **Figure S3a** and **b** show an ADF-STEM image and an identical version of the image overlaid with lines to highlight different surface categories. **Figure S3c** shows the EELS spectra of Li-K edges before and after Li insertion, showing the changes in Li-K edge intensity. The straight lines represent our defined background using a linear function fitted to two regions around the Li-K edge (58–60 and 80–85 eV). The Li distribution can be visualized by extracting the integrated intensity between 60–70 eV.

EELS enables the quantification of atomic concentrations or ratios through the analysis of core-loss spectra. However, an increase in specimen thickness results in a higher probability of plural scattering, consequently reducing the accuracy of quantification. Errors in the detection of elemental

ratios were reported when t/λ (t : sample thickness, λ : mean free path of the incident electron) exceeded approximately 0.5.³ In general, samples with a t/λ value of less than 1.0 are required for quantitative analysis, even when the deconvolution method is used to mitigate the effects of plural scattering. In the context of the current investigation, the t/λ value of our sample was approximately 1.6, which exceeded the optimal range for the quantitative analysis. Therefore, in the present study, a qualitative mapping approach was used, based on the integrated intensity of the Li-K edge. The choice of this thickness aimed to mitigate the surface effects in the TEM samples. As shown in Fig. 2o, the lithiated $\text{Li}_7\text{Ti}_5\text{O}_{12}$ shell was formed three-dimensionally during Li insertion. If the sample thickness was too thin (e.g., the t/λ value was less than 0.5 for quantitative analysis), the core-shell structure would not be observed. Relatively thick samples were used to show the core-shell structure.

SI-3. Electron diffraction

Figure S4 shows the Li distribution and the electron diffraction pattern obtained at the interface between delithiated $\text{Li}_4\text{Ti}_5\text{O}_{12}$ and lithiated $\text{Li}_7\text{Ti}_5\text{O}_{12}$. The selected area for electron diffraction is marked by the circle within the Li distribution. No splitting of spots due to the phase transitions was observed, indicating that phase separation is difficult to detect by electron diffraction.

SI-4. Effect of electron irradiation

When using STEM for the analysis of $\text{Li}_4\text{Ti}_5\text{O}_{12}$, a notable concern is the Li-insertion reactions induced by the high electron dose. Exposure of a high-dose electron beam appears to induce the dissociation of Li-containing compounds on the lamella surface formed during the FIB process, yielding Li ions and electrons and subsequently promoting the rapid growth of a lithiated $\text{Li}_7\text{Ti}_5\text{O}_{12}$ phase at the scanned area.⁴ These reactions are reported to occur at a beam intensity of 2.5×10^5 electron/ \AA^2 and not to occur at a beam intensity of 4.1×10^4 electron/ \AA^2 . Note that the change in the crystal structure from spinel to disordered rock-salt-like phases is reported to occur at a much higher electron beam intensity such as 7.5×10^6 electron/ \AA^2 .⁴ In the present study, the electron dose per Li distribution was 1.1×10^2 electron/ \AA^2 , which was 2–4 orders of magnitude lower than the threshold values. Thus, we believe that changes in the Li concentration and crystal structure hardly occurred in our experiment.

SI-5. Change in Li distribution in another region

Figure S7 shows the change in Li distribution during Li insertion and extraction in another cell. **Figure S7a** and **b** show an ADF-STEM image and an identical version of the image overlaid with color lines highlighting different surface categories. The Li distributions clearly showed the surface Li diffusion at the interface between $\text{Li}_4\text{Ti}_5\text{O}_{12}$ and the current collector (red line). The core-shell structure was observed during Li insertion and not during Li extraction.

Supplementary Figures

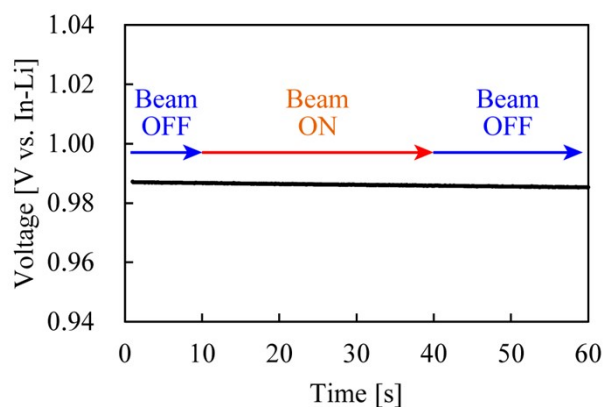


Figure S1. Change in the battery OCV when the electron beam is irradiated to the sample from 10 to 40 seconds.

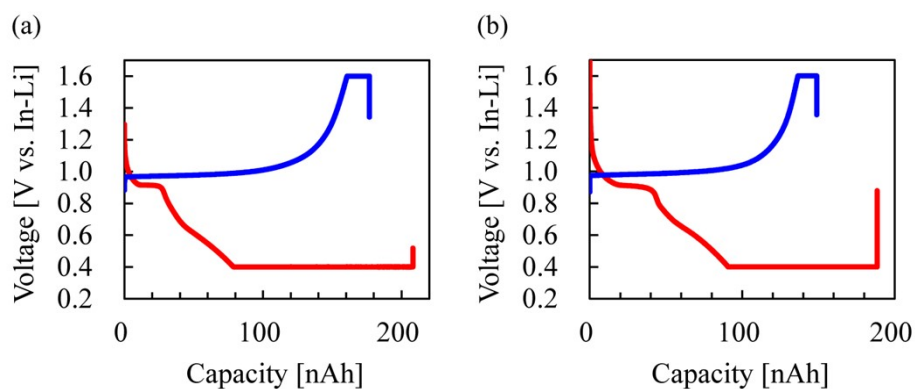


Figure S2. Comparison of charge-discharge curves. (a) Battery cell thinned by FIB with solvent-free silver paste used for the electrical biasing contacts. (b) Bulk battery cell without FIB processing and silver paste.

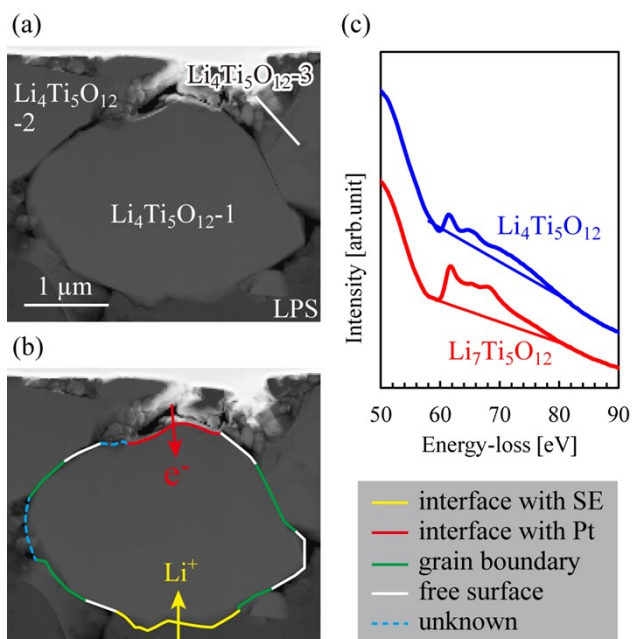


Figure S3. Categories of $\text{Li}_4\text{Ti}_5\text{O}_{12}$ surfaces and method used for visualizing Li distribution. (a) ADF-STEM image presenting Li distributions. (b) ADF-STEM image with color lines highlighting different surface categories. (c) Li-K EEL spectra of delithiated $\text{Li}_4\text{Ti}_5\text{O}_{12}$ (blue) and lithiated $\text{Li}_7\text{Ti}_5\text{O}_{12}$ (red).

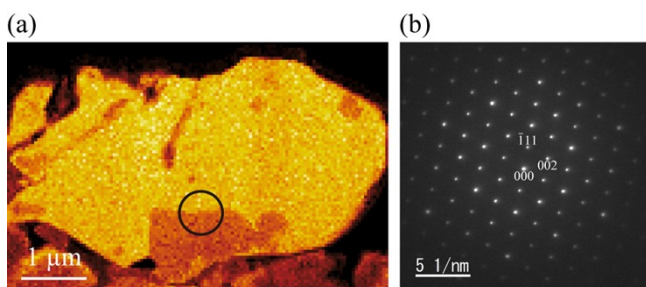


Figure S4. Electron diffraction analysis. (a) Li distribution. (b) Electron diffraction pattern taken along the $[110]$ zone-axis at the interface between delithiated $\text{Li}_4\text{Ti}_5\text{O}_{12}$ and lithiated $\text{Li}_7\text{Ti}_5\text{O}_{12}$. The selected area for electron diffraction is marked by the circle in (a).

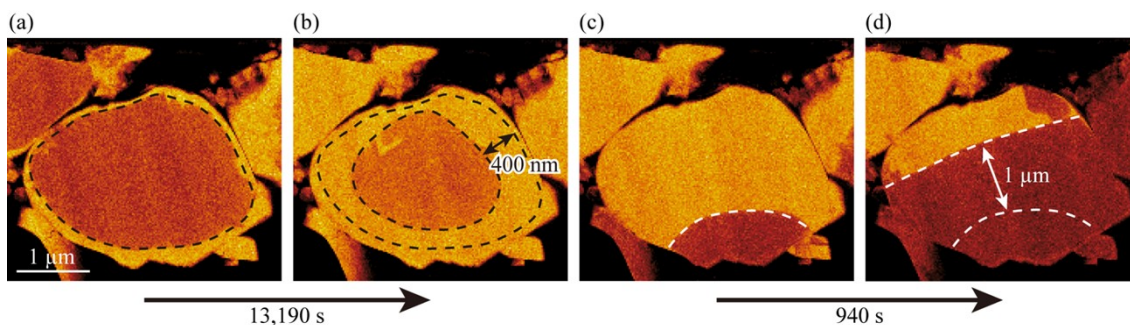


Figure S5. Li diffusion distances and times taken for the diffusion. (a), (b) Li distribution during Li insertion (a) at 150–153 nAh and (b) at 207–208 nAh. (c), (d) Li distribution during Li extraction (c) at 53–78 nAh and (d) at 131–155 nAh.

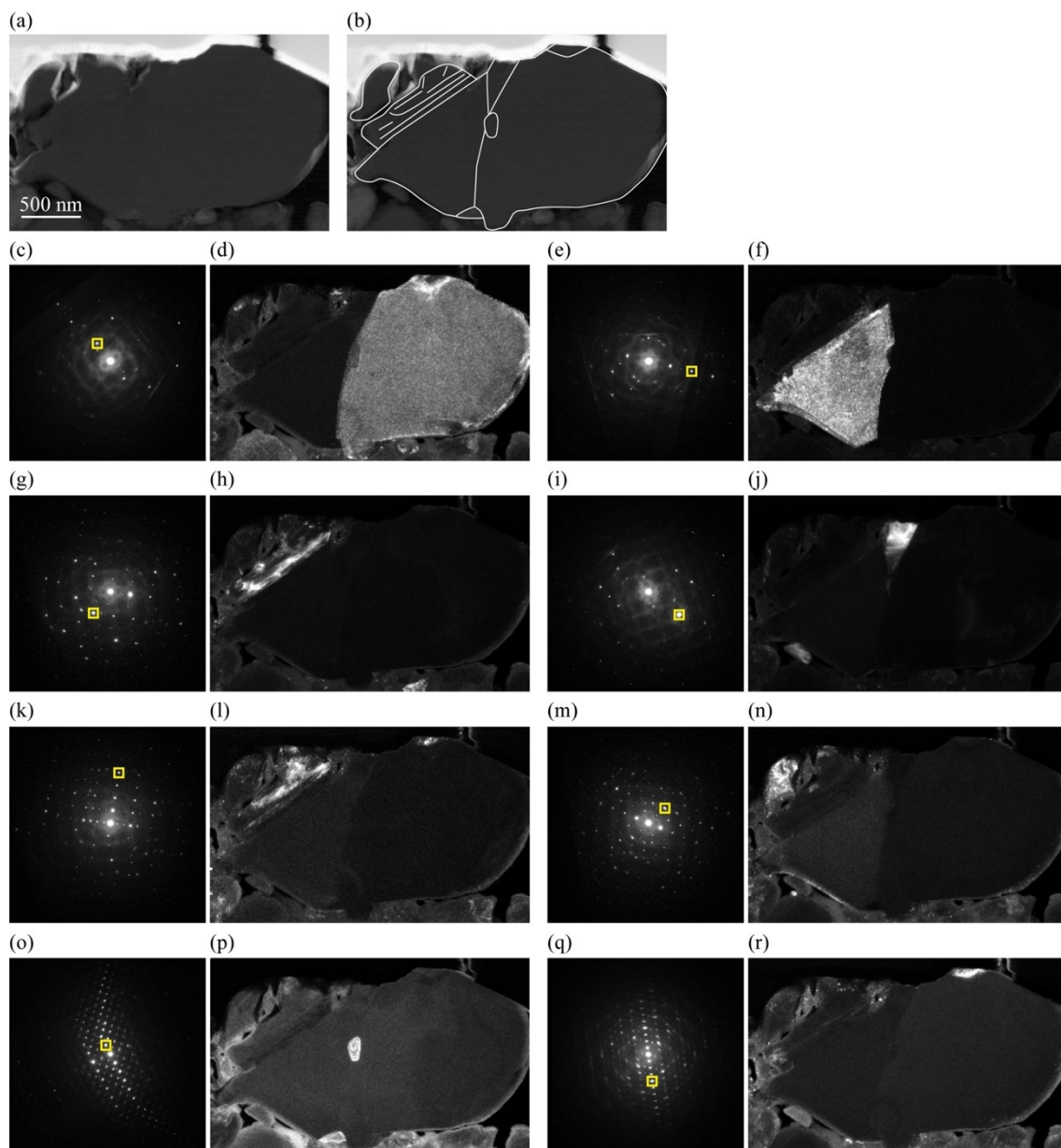


Figure S6. Grain architectures of $\text{Li}_4\text{Ti}_5\text{O}_{12}$ particles visualized by 4D-STEM. (a) ADF-STEM image. (b) ADF-STEM image with lines to highlight $\text{Li}_4\text{Ti}_5\text{O}_{12}$ grains. (c)–(r) Sets of the electron diffraction pattern and intensity map of the diffraction spots indicated by the yellow square in (c), (e), (g), (i), (k), (m), (o), and (q).

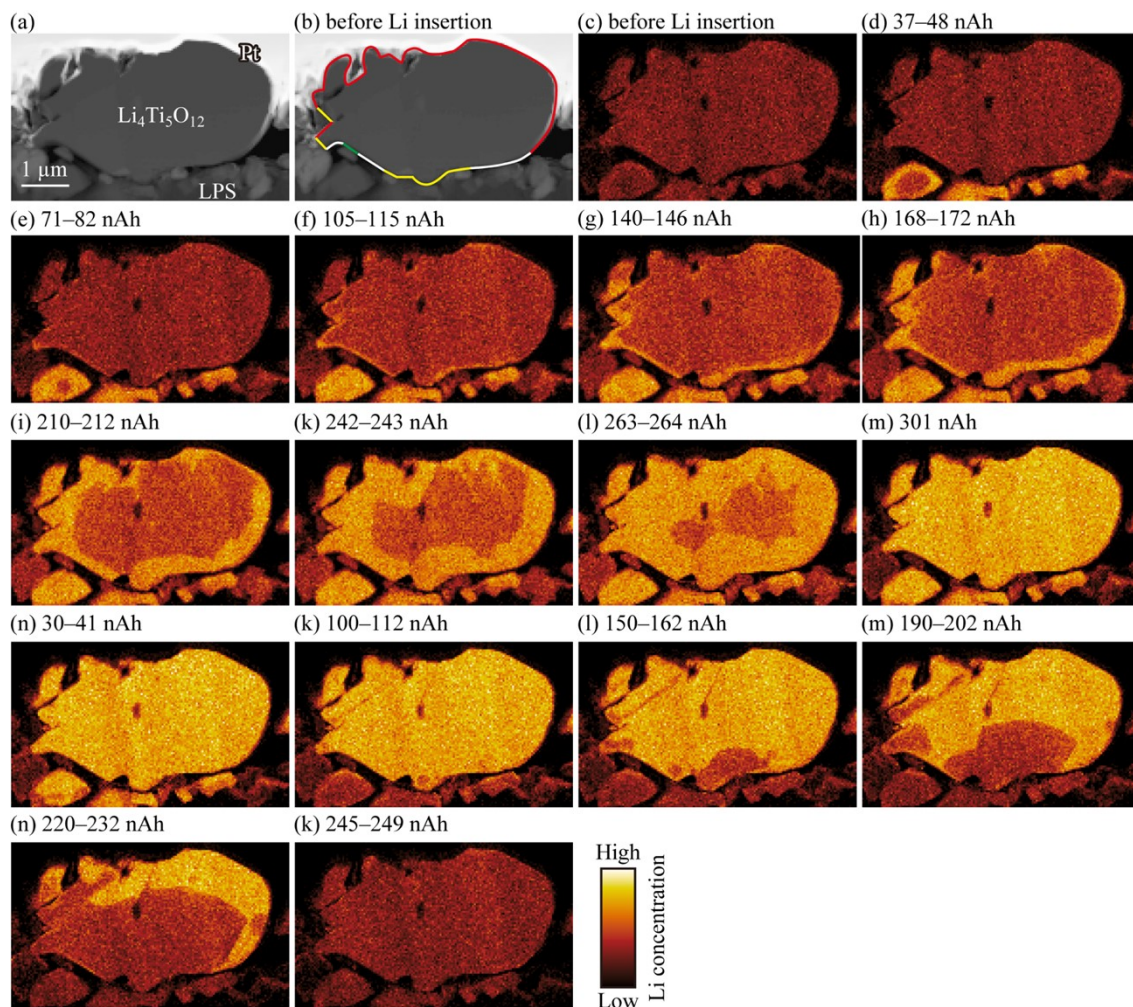


Figure S7. Change in the Li distribution. (a) ADF-STEM image. (b) ADF-STEM image with color lines highlighting different surface categories. (c)–(m) Change in the Li distribution during Li insertion. (n)–(k) Change in the Li distribution during Li extraction. The amount of inserted or extracted Li ions is shown in each panel.

SI-6. References

- 1 Y. Nomura, K. Yamamoto, T. Hirayama, E. Igaki and K. Saitoh, *ACS Energy Lett.*, 2020, **5**, 2098–2105.
- 2 Y. Nomura, K. Yamamoto, M. Fujii, T. Hirayama, E. Igaki and K. Saitoh, *Nat. Commun.*, 2020, **11**, 2824.
- 3 R. F. Egerton, *Electron Energy-Loss Spectroscopy in the Electron Microscope Third Edition*, Springer, New York, 2011.
- 4 M. Kitta and M. Kohyama, *Phys. Chem. Chem. Phys.*, 2017, **19**, 11581–11587.